Photoinduced Melting of a Stripe-Type Charge-Order and Metallic Domain Formation in a Layered BEDT-TTF-Based Organic Salt

S. Iwai,[1,2,*] K. Yamamoto,[3] A. Kashiwazaki,[1] F. Hiramatsu,[1] H. Nakaya,[1] Y. Kawakami,[1] K. Yakushi,[3] H. Okamoto,[4,5] H. Mori,[6] and Y. Nishio[7]

[1]*Department of Physics, Tohoku University, Sendai 980-8578, Japan*
[2]*PRESTO-JST, Kawaguchi 332-0012, Japan*
[3]*Institute of Molecular Science, Okazaki 444-8585, Japan*
[4]*Department of Advanced Materials Science, University of Tokyo, Kashiwa 277-8561, Japan*
[5]*CREST-JST, Kawaguchi 332-0012, Japan*
[6]*Institute of Solid State Physics, University of Tokyo, Kashiwa 277-8561, Japan*
[7]*Department of Physics, Toho University, Chiba 274-8510, Japan*

(Received 14 April 2006; published 1 March 2007)

Photoinduced melting of charge-order (CO) in [bis(ethylenedithiolo)]-tetrathiafulvalene (BEDT-TTF) salts was investigated by femotosecond spectroscopy. Comparative studies on two polytypes exhibiting large [θ-(BEDT-TTF)$_2$RbZn(SCN)$_4$] and small [α-(BEDT-TTF)$_2I_3$] molecular rearrangements through the CO transition were performed. Ultrafast melting of CO for both compounds demonstrates the major contribution of the electronic instability which is due to Coulomb interaction. The roles of the molecular rearrangements on the formation of the CO and the metallic domain are discussed on the basis of low-frequency lattice dynamics.

DOI: 10.1103/PhysRevLett.98.097402 PACS numbers: 78.55.Kz, 73.20.Mf, 78.47.+p

Since the discovery of organic superconductors, layered [bis(ethylenedithiolo)]-tetrathiafulvalene (BEDT-TTF)-based salts with a 1/4-filled hole band have attracted much attention as typical organic correlated electron systems [1–4]. A recent central issue regarding these salts is a stripe-type charge-order (CO), which is realized by long-range Coulomb repulsion [2–5]. Precise structural analysis [5–7] and thermodynamic measurements [8–10] on the layered salts with COs revealed that the electron-lattice interaction, or, equivalently, the molecular rearrangements modulating the intermolecular charge transfer (CT) interaction, also plays an important role in the stabilization of the CO. The contribution of such molecular rearrangement on the CO depends on the polytype with different crystal structures, which are characterized by θ, α, β, ... [3,4], and so on.

Very recently, the gigantic and nonlinear electric responses of the COs to an electric field and light have been assessed for the (BEDT-TTF) salts [11,12] from the perspective of their potential applications to organic devices. These novel responses are attributable to nonequilibrium insulator-to-metal (I-M) transitions, although their mechanism has not yet been understood. From the scientific point of view, it is of great interest to clarify the interplay between the Coulomb repulsion and the molecular rearrangement in the nonequilibrium I-M transition, since they are key factors for the stabilization of the COs.

Femtosecond pump-probe (PP) spectroscopy is an effective method for investigating the nonequilibrium phase transitions [13]. Until now, this method has been applied on several typical Peierls or spin-Peierls systems, and the characteristic photoinduced phase transitions (PIPTs), which are driven by structural instability, have indeed been observed [14–17]. Using this method, the most fundamental problem of the PIPT in the CO system, i.e., the clarification of the roles of Coulomb interactions and the molecular rearrangements to the COs, is expected to be achieved. Comparative studies on the polytypes of BEDT-TTF salts having different molecular rearrangements are available for the investigation of the problem.

In this Letter, we report PIPTs in BEDT-TTF salts θ-(BEDT-TTF)$_2$RbZn(SCN)$_4$ (θ-RbZn) [5] and α-(BEDT-TTF)$_2I_3$ (α-I_3) [18], which were studied using femtosecond midinfrared (MIR) PP spectroscopy. These salts commonly show the COs at a temperature less than T_c (T_c = 195 K for θ-RbZn and T_c = 135 K for α-I_3). They indicate large (θ-RbZn) [5,6,10] and small (α-I_3) [7–10] molecular rearrangements in the CO phases as shown in Figs. 1(a) and 1(b), respectively. Ultrafast CO melting was observed for both compounds, representing the major contribution of the electronic instability due to the Coulomb interaction. However, excitation intensity (I_{ex})-dependent relaxation dynamics of the metallic state and the low-frequency coherent phonons show a non-negligible contribution of the molecular rearrangements to the melting of the COs and the stabilization of the metallic state.

Single crystals of θ-RbZn and α-I_3 were prepared using reported procedures [5,18]. A Ti:sapphire regenerative amplifier operating at 1 kHz (Hurricane; Spectra-Physics) was used for femtosecond PP reflection spectroscopy, with a handmade dual optical parametric amplifier system used as a light source. The time resolution of the system was ca. 200 fs.

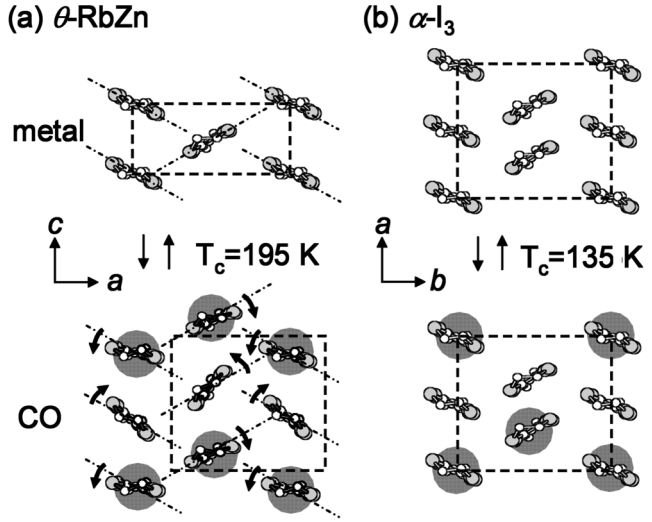

FIG. 1. (a),(b) Schematic representations of the molecular arrangement of (a) θ-RbZn and (b) α-I_3. Solid gray circles indicate the localized charge (charge rich site) of CO. Dashed rectangles indicate the unit cell.

Figures 2(a) and 2(c) show the polarized reflectivity spectra of θ-RbZn and α-I_3 for the electric field of light perpendicular to the molecular stack (the c axis in θ-RbZn and the a axis in α-I_3 as shown in Fig. 1). A reflection band located below 0.8 eV was assigned to the CT transition between the BEDT-TTF molecules. Reflectivity spectra for temperatures $T > T_c$ and $T < T_c$ are represented by dashed and solid curves, respectively. Comparison of the reflectivity spectra in the MIR region with the behaviors of the transport [5,18] suggests that the MIR spectrum is very sensitive to the I-M transition in these compounds, although the spectrum in a far-infrared region is more

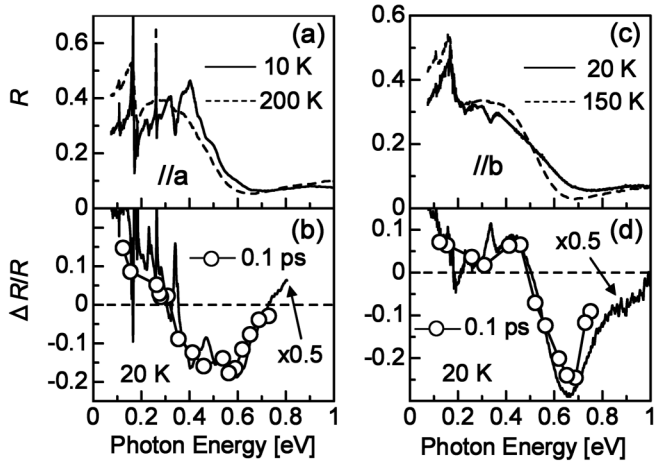

FIG. 2. (a),(c) Reflectivity spectra of (a) θ-RbZn and (c) α-I_3. (b),(d) $\Delta R/R$ spectra measured at $\tau_d = 0.1$ ps (20 K) are shown as open circles. E_{ex} and I_{ex} are 0.89 eV and 0.1 mJ cm^{-2}, respectively. Differential spectra $(R_M - R_I)/R_I$ are represented as solid curves.

sensitive to the generation of the metallic state. The open circles in Figs. 2(b) and 2(d) show the transient reflectivity ($\Delta R/R$) spectra at 20 K. The pump ($E_{ex} = 0.89$ eV) and probe lights were polarized perpendicular to the molecular stack. The $\Delta R/R$ spectra measured at t_d (the delay time of the probe light after excitation) $= 0.1$ ps are analogous to the differential reflectivity spectra $(R_M - R_I)/R_I$ [solid curves in Figs. 2(b) and 2(d)], in which R_M and R_I represent the reflectivity of the metallic and CO insulator phases, respectively. This indicates that the melting of the CO and the formation of the metallic state occur immediately after the photoexcitation in both compounds. The magnitude of $\Delta R/R$ observed at 0.1–0.8 eV for $t_d = 0.1$ ps increases linearly with I_{ex} up to 0.1 mJ cm^{-2}. Considering the absorption coefficients [15 000 cm^{-1} (θ-RbZn), 5000 cm^{-1} (α-I_3)] at 0.89 eV and unit cell volumes (2050 Å^3 for θ-RbZn, 1690 Å^3 for α-I_3), the I_{ex} of 0.1 mJ cm^{-2} corresponds to the excitation of one photon per approximately 1600 (θ-RbZn) and 600 (α-I_3) donor molecules. The efficiency of the photoinduced metallic state is evaluated as 100 (θ-RbZn) and 250 (α-I_3) molecules/photon. The ultrafast melting of the CO for both θ-RbZn and α-I_3 suggests that these responses are not driven by the structural instability, being different from that in Peierls and spin-Peierls systems [15–17]. However, the drastic changes in the electronic states, that is, the melting of the CO and the formation of the metallic state, necessarily cause finite molecular rearrangements. In order to discuss the supporting role of these structural changes, we investigate the I_{ex} dependence of the relaxation dynamics of the metallic state and the coherent phonons produced by the changes of the electronic states.

Figures 3(a)–3(d) show the time evolutions of $\Delta R/R$ at 0.12 eV [(a) θ-RbZn (20 K), (b) α-I_3 (20 K), and (c),(d) α-I_3 (124 K)] for various I_{ex} values. Decay profiles reflecting the recovery of CO for θ-RbZn [Fig. 3(a)] were fitted using a two-component exponential curve whose decay times (fractions) are 0.2 (0.73) and 2 ps (0.17). Results show that the recovery dynamics are independent of I_{ex} (0.001–0.1 mJ cm^{-2}) and temperature (20–150 K). On the other hand, the decay profiles of α-I_3 depend strongly on I_{ex} and temperature. Figure 3(b) shows that the decay time of the dominant component lengthens with I_{ex} in the picosecond region. At 124 K, just below T_c, the decay time increases more markedly with I_{ex} from the subpicosecond to the nanosecond time domain, as shown in Figs. 3(c) and 3(d). The longer decay time for the larger I_{ex} near T_c suggests the cooperative nature and critical slowing down (CSD) of the photogenerated quasistable semimacroscopic metallic state in α-I_3. These results can be related with the difference in the degree of structural modification in the thermal I-M transition. That is, in the CO phase of θ-RbZn, the structural symmetry is reduced by the molecular rotation [6] [Fig. 1(a)], modulating the intermolecular CT, while such structural modification is very small in α-I_3

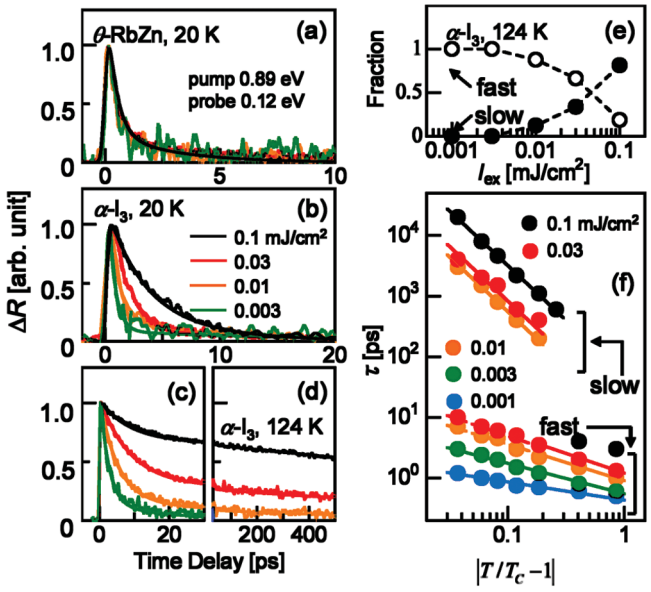

FIG. 3 (color). (a)–(d) Time evolutions of $\Delta R/R$ observed at 0.12 eV in (a) θ-RbZn (20 K) and in α-I_3 [(b) 20 K, (c),(d) 124 K] for various I_{ex}. The fitting curves (see text) are also shown. (e) The fraction of the fast (open circles: τ_{fast} ca. 1 ps) and slow (solid circles: τ_{slow} ca. 1 ns) decay components in α-I_3 are plotted as a function of I_{ex} (124 K). (f) Relaxation times of the metallic states τ_{fast} and τ_{slow} are plotted as a function of $|T/T_C - 1|$ for various I_{ex}.

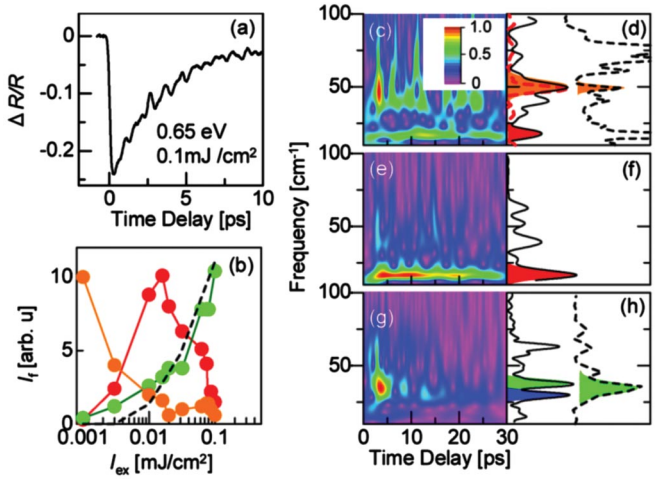

FIG. 4 (color). (a) Time evolution of $\Delta R/R$ for α-I_3 (20 K). (b) Normalized Fourier intensity (I_f) at 48 cm^{-1} (orange dot, $\times 20$), 17 cm^{-1} (red dot), and 38 cm^{-1} (green dot, $\times 2$) is plotted as a function of I_{ex}. The dashed curve represents the fraction of τ_{slow} in Fig. 3(e). (c), (e), and (g) Wavelet contour maps of oscillation frequencies for (c) 0.001, (g) 0.01, and (e) 0.1 mJ cm^{-2}. The corresponding Fourier power spectra are shown, respectively, in (d), (f), and (h). The Fourier spectrum of the coherent oscillation (20 K) and steady state Raman spectrum (10 K) in θ-RbZn are also shown as red and black dashed curves in (d), respectively. The dashed curve in (h) shows the Fourier spectrum of the coherent oscillation of the metallic phase for $T > T_c$.

[7–10] [Fig. 1(b)]. Considering the large molecular rearrangement and the hysteresis of the specific heat observed in θ-RbZn [9,10], the large potential barrier against the molecular rotation might block the generation of semimacroscopic quasistable metallic domains in θ-RbZn. Consequently, the microscopic unstable metallic domains return to the CO states within a few picoseconds. On the other hand, the small structural difference and the small barrier between the CO and metallic phases in α-I_3 allow the stabilization of the metallic domains.

Figure 4(a) shows the time evolution of $\Delta R/R$ observed at 0.65 eV in α-I_3. For probe energies near the CT band, the oscillatory structures are clearly observed in both compounds. It is noteworthy that the oscillatory profile depends strongly on I_{ex} in α-I_3, while such I_{ex} dependence was not observed in θ-RbZn. Figures 4(c), 4(e), and 4(g) show the contour maps obtained by the continuous wavelet transformation for typical values of I_{ex} (0.001, 0.01, and 0.1 mJ cm^{-2}). The corresponding Fourier power spectra exhibit the various oscillatory components depending on I_{ex} values as seen in Figs. 4(d), 4(f), and 4(h). For the small excitation intensity ($I_{ex} = 0.001$ mJ cm^{-2}), the frequency of the dominant oscillation band shown by the orange shading in Fig. 4(d) is 48 cm^{-1}, which is almost equal to that of the coherent oscillation in θ-RbZn [the red dashed curve in Fig. 4(d)]. This is also in agreement with the frequency of the steady state Raman peak observed only at $T < T_c$ in θ-RbZn [dashed curve in Fig. 4(d)]. Therefore, the 48 cm^{-1} oscillation is ascribed to the ground state mode of BEDT-TTF, which stabilizes the CO. With increasing I_{ex}, the lower-frequency (17 cm^{-1}) band indicated by the red shading appears at $I_{ex} = 0.01$ mJ cm^{-2} as seen in Fig. 4(f). For $I_{ex} = 0.1$ mJ cm^{-2}, the 29 cm^{-1} band (blue shading) and the 38 cm^{-1} band (green shading) become dominant as seen in Fig. 4(h). Normalized Fourier intensities (I_f) observed at 48, 17, and 38 cm^{-1} were plotted as a function of I_{ex} in Fig. 4(b). The 38 cm^{-1} mode observed for the large I_{ex} in α-I_3 is considered to stabilize the semimacroscopic metallic domain for the following reason. The photoexcitation of the metallic phase for $T > T_c$ also generates the coherent oscillation after the ultrafast relaxation of the photoexcited state (not shown). The Fourier spectrum of this oscillating component is shown by the dashed curve in Fig. 4(h), indicating that the oscillation frequency is close to 38 cm^{-1}. Therefore, the 48 and 38 cm^{-1} modes are associated with CO melting and the stabilization of the semimacroscopic metallic domain, respectively. The 17 and 29 cm^{-1} modes are considered to be due to the CO state which is affected by the neighboring photogenerated metallic domains. Nevertheless, the period of these low frequency modes is much slower than the rise time (<200 fs) of the reflectivity change reflecting the formation of the metallic state. This clearly shows that the melting of the CO and the formation

of the metallic state are not dominated by these structural changes.

Next, we discuss the semimacroscopic nature of the metallic domain in α-I_3 on the basis of the CSD. The temperature dependence of the decay time of $\Delta R/R$ τ_{fast} and τ_{slow} are plotted as functions of reduced temperature $|T/T_C - 1|$ for various I_{ex} values in Fig. 3(f). τ_{fast} and τ_{slow} represent the time constant obtained by the fitting procedure, using three exponential functions whose time constants are $\tau_{\mathrm{fast}} \sim 1$ ps, $\tau_{\mathrm{middle}} \sim 15$ ps, and $\tau_{\mathrm{slow}} \sim 1$ ns. Of the three components, the decay time of the small ($\sim$5%) component $\tau_{\mathrm{middle}} \sim 15$ ps is independent of temperature, indicating that τ_{middle} does not concern the I-M transition. As seen in Fig. 3(f), for $T < T_c$, τ_{fast} and τ_{slow} increase with $|T/T_C - 1|$ divergently. We plotted the I_{ex} dependence of the fraction for the fast and slow components in Fig. 3(e). The fast component was observed solely for small I_{ex}, while the slow component becomes dominant for large I_{ex}.

According to the dynamic scaling theory of the second-order transition, the CSD observed in the relaxation time (τ) of the quasistable state can be represented by $\tau \propto |T/T_C - 1|^{-\nu z}$ [19], where ν and z are critical exponents of the correlation length ξ and the dynamic critical exponent, respectively. For $I_{\mathrm{ex}} > 0.01$ mJ cm^{-2}, τ_{slow} shows $\nu z = 1.8$, which is close to the calculated value ($=2.1665$) as evaluated by Monte Carlo simulation within the framework of the two-dimensional (2D) Ising model [20]. The slow component is, therefore, attributable to the semimacroscopic metallic domain. The I_{ex} dependence of the fraction of τ_{slow} showing $\nu z = 1.8$ [the solid black circles in Fig. 3(e) and the dashed curve in Fig. 4(b)] is similar to that of I_{f} at 38 cm^{-1} [the solid green circles in Fig. 4(b)]. This fact also indicates that the 38 cm^{-1} mode is again attributable to the semimacroscopic metallic domain. On the other hand, νz for τ_{fast} is evaluated to be from 0.3 (0.001 mJ cm^{-2}) to 0.65 (0.03 mJ cm^{-2}), which is much smaller than the calculated value. It would be related to the fact that the photoinduced state for the weak excitation intensity is regarded as the microscopic metallic domains in the CO background.

In summary, we investigated the dynamics of photoinduced melting of CO and I-M transition in BEDT-TTF salts θ-(BEDT-TTF)$_2$RbZn(SCN)$_4$ (θ-RbZn) and α-(BEDT-TTF)$_2I_3$ (α-I_3). Ultrafast and efficient photogeneration of a metallic state was observed for both compounds, showing the major contribution of electronic instability. The dynamics of the metallic state are, however, clearly different; i.e., local melting of CO engenders ultrafast recovery in θ-RbZn, whereas the 2D semimacroscopic metallic domain showing critical slowing down is generated in α-I_3. The excitation intensity dependences of the relaxation dynamics of the metallic state and the observed coherent phonons indicate that the molecular rearrangements also play important roles on the I-M transition of the present systems.

*Electronic address: s.iwai@sspp.phys.tohoku.ac.jp

[1] T. Ishiguro, Y. Yamaji, and G. Saito, *Organic Super Conductors* (Springer, Berlin, 1997).
[2] S. Mazumdar, R. T. Clay, and D. K. Campbell, Phys. Rev. B **62**, 13 400 (2000).
[3] H. Seo, C. Hotta, and H. Fukuyama, Chem. Rev. **104**, 5005 (2004).
[4] M. Dressel and N. Drichko, Chem. Rev. **104**, 5689 (2004).
[5] H. Mori, S. Tanaka, and T. Mori, Phys. Rev. B **57**, 12 023 (1998).
[6] M. Watanabe, Y. Noda, Y. Nogami, and H. Mori, J. Phys. Soc. Jpn. **73**, 116 (2004).
[7] T. Kakiuchi and H. Sawa (private communication).
[8] N. A. Fortune, K. Murata, M. Ishbashi, M. Tokumoto, N. Kinoshita, and H. Anzai, Solid State Commun. **79**, 265 (1991).
[9] C. P. Heidmann, A. Barnsteiner, F. Groß-Allatg, B. S. Chandrasekhar, and E. Hess, Solid State Commun. **84**, 711 (1992).
[10] Y. Nishio (to be published). The hysteresis of the specific heat was evaluated to be 40 K (θ-RbZn) and $<$0.2 K (α-I_3) using the differential thermal-analysis method with a scan speed of 0.52 K min^{-1}.
[11] F. Sawano, I. Terasaki, H. Mori, M. Watanabe, N. Ikeda, Y. Nogami, and Y. Noda, Nature (London) **437**, 522 (2005).
[12] N. Tajima, J. Fujisawa, N. Naka, T. Ishihara, R. Kato, Y. Nishio, and K. Kajita, J. Phys. Soc. Jpn. **74**, 511 (2005).
[13] Special topics on Photo-Induced Phase Transition and Their Dynamics, edited by M. Gonokami and S. Koshihara [J. Phys. Soc. Jpn. **75**, 01101 (2006)].
[14] A. Cavalleri, Th. Dekorsky, H. H. W. Chong, J. C. Kieffer, and R. W. Schoenlein, Phys. Rev. B **70**, 161102 (2004).
[15] H. Okamoto, Y. Ishige, S. Tanaka, H. Kishida, S. Iwai, and Y. Tokura, Phys. Rev. B **70**, 165202 (2004).
[16] M. Chollet, L. Guerin, N. Uchida, S. Fukaya, H. Shimada, T. Ishikawa, K. Matsuda, T. Hasegawa, A. Ohta, H. Yamochi, G. Saito, R. Tazaki, S. Adachi, and S. Koshihara, Science **307**, 86 (2005).
[17] H. Okamoto, K. Ikegami, T. Wakabayashi, Y. Ishige, J. Togo, H. Kishida, and H. Matsuzaki, Phys. Rev. Lett. **96**, 037405 (2006).
[18] K. Bender, I. Henning, D. Schweitzer, K. Dietz, H. Endre, and H. J. Keller, Mol. Cryst. Liq. Cryst. **108**, 359 (1984).
[19] P. C. Hohenberg and B. I. Hailerin, Rev. Mod. Phys. **49**, 435 (1977).
[20] M. P. Nightingale and H. W. J. Blote, Phys. Rev. Lett. **76**, 4548 (1996).